Submitted to the Astrophysical Journal
Preprint typeset using LaTeX style emulateapj v. 10/09/06

A STIS SURVEY FOR O VI ABSORPTION SYSTEMS AT $0.12 < Z \lesssim 0.5$ I.: THE STATISTICAL PROPERTIES OF IONIZED GAS[1]

Christopher Thom and Hsiao-Wen Chen
Dept. of Astronomy & Astrophysics, 5640 S. Ellis Ave, Chicago, IL, 60637, U.S.A.
cthom,hchen@oddjob.uchicago.edu

Submitted to the Astrophysical Journal

ABSTRACT

We have conducted a systematic survey for intervening O VI absorbers in available echelle spectra of 16 QSOs at $z_{\rm QSO} = 0.17 - 0.57$. These spectra were obtained using HST/STIS with the E140M grating. Our search uncovered a total of 27 foreground O VI absorbers with rest-frame absorption equivalent width $W_r(1031) \gtrsim 25$ mÅ. Ten of these QSOs exhibit strong O VI absorbers in their vicinity. Our O VI survey does not require the known presence of Lyα, and the echelle resolution allows us to identify the O VI absorption doublet based on their common line centroid and known flux ratio. We estimate the total redshift survey path, Δz, using a series of Monte-Carlo simulations, and find that $\Delta z = 1.66, 2.18$, and 2.42 for absorbers of strength $W_r = 30, 50$ and 80 mÅ, respectively, leading to a number density of $d\mathcal{N}(W \geq 50\ {\rm m\AA})/dz = 6.7 \pm 1.7$ and $d\mathcal{N}(W \geq 30\ {\rm m\AA})/dz = 10.4 \pm 2.2$. In contrast, we also measure $d\mathcal{N}/dz = 27 \pm 9$ for O VI absorbers of $W_r > 50$ mÅ at $|\Delta v| < 5000$ km s^{-1} from the background QSOs. Using the random sample of O VI absorbers with well characterized survey completeness, we estimate a mean cosmological mass density of the O VI gas $\Omega({\rm O}^{5+})\, h = (1.7 \pm 0.3) \times 10^{-7}$. In addition, we show that $< 5\%$ of O VI absorbers originate in underdense regions that do not show a significant trace of H I. Furthermore, we show that the neutral gas column N(H I) associated with these O VI absorbers spans nearly five orders of magnitude, and shows moderate correlation with N(O VI). Finally, while the number density of O VI absorbers varies substantially from one sightline to another, it also appears to be inversely correlated with the number density of H I absorbers along individual lines of sight.

Subject headings: cosmology: observations—intergalactic medium—quasars: absorption lines

1. INTRODUCTION

Uncovering the missing baryons in the present-day universe is one of the central issues in observational cosmology, because an accurate accounting of the baryon budget at different locations sets an important constraint in modeling galaxy formation and evolution. Over the past few years, measurements of the baryonic mass density from independent methods have approached a consistent value with high precision, $\Omega_b\, h^2 = 0.020 \pm 0.002$ (Burles et al. 2001; Spergel et al. 2003; Wang et al. 2003; O'Meara et al. 2006). But while $> 95\%$ of all baryons can be accounted for in the Lyα forest at redshift $z \sim 3$ (Rauch et al. 1997), only 1/3 have been identified at redshift $z = 0$ in known components, such as stars and neutral gas in galaxies or hot plasma in galaxy clusters (e.g. Persic & Salucci 1992; Fukugita et al. 1998).

Cosmological simulations indicate that $\approx 30 - 40\%$ of all baryons at the present epoch reside in a diffuse warm-hot intergalactic medium (WHIM), with temperatures in the range $10^5 < T < 10^7$ K, rather than in virialized halos where galaxies or galaxy groups lie (Cen & Ostriker 1999; Davé et al. 2001). The simulations also show that this WHIM is shock-heated as tenuous gas accretes onto large-scale filamentary structures and remains hot owing to the low gas density and inefficient cooling. Locating the WHIM in order to verify these models is difficult, because the temperature of the gas is too low to be easily detected with the current generation of x-ray satellites and is too hot to be observed from the ground using optical-IR facilities. Simple ionization modeling of hot gas at $T \sim 3 \times 10^5$ K and metallicity 0.1 solar has shown that the gaseous clouds would imprint prominent absorption features produced by ionic transitions such as O VI $\lambda\lambda$ 1031, 1037 and Ne VIII $\lambda\lambda$ 770, 780 in the spectra of background QSOs (e.g. Verner et al. 1994; Mulchaey et al. 1996). Surveys for the WHIM based on the presence of these ions at $z < 1$ therefore require a high-resolution UV spectrograph in space.

Tripp et al. (2000) searched for intervening O VI absorbers along the sightline toward H1821+643 ($z_{\rm QSO} = 0.297$) in echelle spectra ($R \equiv \lambda/\Delta\lambda \approx 43,000$) obtained using the Space Telescope Imaging Spectrograph (STIS) on board the Hubble Space Telescope (HST). The search indicated that intervening O VI absorption systems found in QSO spectra may indeed contain a significant fraction of baryons that had been missed by surveys based on the direct detection of photons emitted by known objects. Subsequent searches along individual sightlines have been carried out toward PG0953+415 at $z_{\rm QSO} = 0.239$ (Savage et al. 2002), PG1259+593 at $z_{\rm QSO} = 0.478$ (Richter et al. 2004); PG1116+215 at $z_{\rm QSO} = 0.1765$ (Sembach et al. 2004), PKS0405−123 at $z_{\rm QSO} = 0.573$ (Prochaska et al. 2004), and HE0226−4110 at $z_{\rm QSO} = 0.495$ (Lehner et al. 2006). The measured line density of intervening O VI absorbers with rest-frame absorption equivalent width of the 1031 transition $W_r \geq 50$ mÅ ranges from $d\mathcal{N}$(O VI)$/dz = 11$

[1] Based in part on observations with the NASA/ESA Hubble Space Telescope, obtained at the Space Telescope Science Institute, which is operated by the Association of Universities for Research in Astronomy, Inc., under NASA contract NAS5–26555.

to 36[2] per line of sight at $z_{\rm O\,VI} = [0, 0.5]$.

The large scatter in the observed number density of O VI absorbers suggests a significant variation in the spatial distribution of O^{5+} ions across different sightlines. It also underscores a potential systematic bias in evaluating the cosmological mass density of warm-hot gas based on selective quasar sightlines. The first blind search of O VI absorbers was carried out at $z_{\rm O\,VI} = [0.5, 2.1]$ toward 11 background quasars by Burles & Tytler (1996) using medium resolution ($R \approx 1300$) and $S/N \approx 20$ Faint Object Spectrograph spectra. They reported $d\mathcal{N}({\rm O\,VI})/dz = 1.0 \pm 0.6$ per line of sight at a mean redshift $\langle z_{\rm O\,VI}\rangle = 0.9$ with $W_r \geq 210$ mÅ. More recently, Danforth & Shull (2005) conducted a search of O VI absorption features in *known* Lyα absorbers at $z_{\rm abs} < 0.15$, using Far Ultraviolet Spectroscopic Explorer (FUSE) spectra ($R \approx 15,000$) of 31 active galactic nuclei (AGN). Their search yielded $d\mathcal{N}({\rm O\,VI})/dz = 9 \pm 2$ and 17 ± 3 per line of sight with $W_r \geq 50$ and $W_r \geq 30$ mÅ, respectively, at $z_{\rm O\,VI} < 0.15$, which is lower than measurements from individual lines of sight discussed earlier.

Despite the large scatter in the number density of intervening O VI absorbers, these measurements imply that at least $\sim 10\%$ of the total baryons reside in the gaseous clouds probed by the O VI transition. Assuming a mean metallicity of 1/10 solar and an ionization fraction of 20% for the O VI absorbers, Tripp et al. (2000) derived a lower limit to the cosmological mass density in the ionized gas of $\Omega_b({\rm O\,VI}) \gtrsim 0.003\,h^{-1}$ and Danforth & Shull (2005) derived $\Omega_b({\rm O\,VI}) \approx 0.002\,h^{-1}$. This general inference of O VI absorbers being a substantial reservoir of missing baryons is supported by numerical simulations that result in a mean metallicity of 1/10 solar for the WHIM (Cen et al. 2001; Fang & Bryan 2001). However, additional uncertainties arise due to the unknown ionization state and metallicity of the gas.

We have conducted a systematic survey of intervening O VI absorbers in available echelle spectra obtained using HST/STIS with the E140M grating. A search of the HST data archive yielded high-resolution ($R \approx 45,000$) spectra of 16 distant quasars at $z_{\rm QSO} = 0.17 - 0.57$ with a mean $S/N > 7$ per resolution element. These quasars have been selected by different authors for different studies and have bright UV fluxes that are suitable for STIS echelle observations. Therefore, they represent a random, flux-limited sample of quasar spectra for an unbiased search of intervening absorbers. The entire STIS echelle spectroscopic sample of quasars summarized in Table 1 defines the random sightlines along which our blind search of intervening O VI absorbers was conducted.

The primary objectives of the blind O VI survey are: (1) to obtain a statistically representative sample of O VI absorbers along random lines of sight for an accurate measurement of the cosmological mass density of warm-hot gas at low redshift; and (2) to study the incidence of O VI absorbers along individual sightlines for quantifying the spatial variation of O VI absorbing gas. These O VI absorbers identified along random sightlines also form a uniform sample for studying the physical nature of tenuous gas probed by the presence of O^{5+} and for investigating their large-scale galactic environment. Here we focus our discussion on the statistical properties of O VI absorbers. Studies of the gas properties and discussions of individual absorbers are given in an accompanying paper (Thom & Chen, 2008; hereafter paper II), and studies of the surrounding galaxies will be presented in future papers.

This paper is organized as follows. In Section 2, we summarize the available quasar spectra and the data quality. In Section 3, we describe our approach for identifying an O VI $\lambda\lambda$ 1031, 1037 absorption doublet with no prior knowledge of the presence of H I or other ionic transitions. A Monte-Carlo analysis was performed for evaluating the completeness of the survey. In Section 4, we present a statistical sample of O VI absorbers identified along the sightlines toward the 16 background quasars. We measure different statistical quantities of the ionized gas. In Section 5, we compare our search results with others and discuss the implications in Section 6. We adopt a Λ cosmology, $\Omega_{\rm M} = 0.3$ and $\Omega_\Lambda = 0.7$, with a dimensionless Hubble constant $h = H_0/(100\ {\rm km\ s^{-1}\ Mpc^{-1}})$ throughout the paper.

2. THE STIS ECHELLE SPECTRA

The goal of our project is to conduct a blind survey of O VI $\lambda\lambda$ 1031, 1037 absorption doublet features along random lines of sight toward background quasars for establishing a statistically representative sample of the O VI absorbers at $z < 0.5$. The survey therefore requires high-quality UV spectra of distant quasars. In addition, we focused our search on available echelle quality spectra in order to uncover the majority of O VI absorbing gas. Both numerical simulations presented by Chen et al. (2003) and the recent FUSE survey by Danforth & Shull (2005) show that the bulk ($> 60\%$) of O VI absorbers have rest-frame absorption equivalent width of the 1031 transition $W_r = 30 - 100$ mÅ. An echelle spectrum with resolution element $\delta\,v \approx 7$ km s^{-1} at moderate S/N (≈ 5) per resolution element is therefore necessary for detecting these weak lines. This criterion excludes Faint Object Spectrograph data (typically $\delta\,v \approx 230 - 270$ km s^{-1}) from our search. Finally, the throughput of STIS declines steeply at $\lambda < 1180$ Å, corresponding to a minimum $z_{\rm O\,VI} \approx 0.14$, and we therefore include in our sample only those sightlines toward quasars at $z_{\rm QSO} \gtrsim 0.16$ for the search of intervening O VI absorbers.

Our search in the HST data archive yielded 16 quasars observed with the STIS E140M grating. A summary of the STIS observations is presented in Table 1, where we list in columns (1)–(6), the QSO field, $z_{\rm QSO}$, minimum and maximum redshifts over which the sample of random O VI absorbers is established ($z_{\rm min}$, $z_{\rm max}$), total exposure time, and the program ID. We note that $z_{\rm max}$ is defined for O VI absorbers at velocity separation > 5000 km s^{-1} from the background QSO, but the line search is conducted through the emission redshift of the QSO. Individual flux-calibrated spectra were processed using the latest calibration files (Aloisi et al. 2005) and retrieved from the MAST server. For each QSO, individual echelle

[2] Tripp et al. (2000) reported $d\mathcal{N}({\rm O\,VI})/dz \sim 48$ based on four O VI absorbers found with $W_r > 30$ mÅ toward H1821+643. Three of the four absorbers have $W_r > 50$ mÅ. We therefore scale $d\mathcal{N}({\rm O\,VI})/dz$ accordingly and work out $d\mathcal{N}({\rm O\,VI})/dz = 36$ for O VI absorbers stronger than $W_r = 50$ mÅ.

TABLE 1
Summary of the STIS Echelle Spectra

QSO (1)	$z_{\rm QSO}$ (2)	$z_{\rm min}$ (3)	$z_{\rm max}$[a] (4)	$t_{\rm exp}$ (5)	PID (6)
HE 0226-4110	0.4950	0.1154	0.4707	43772	9184
PKS 0312-77	0.2230	0.1241	0.1999	37908	8651
PKS 0405-12	0.5726	0.1241	0.5478	27208	7576
HS 0624+6907	0.3700	0.1222	0.3464	61950	9184
PG 0953+415	0.2390	0.1144	0.2163	24478	7747
3C 249.1	0.3115	0.1222	0.2885	68776	9184
PG 1116+215	0.1765	0.1144	0.1536	39836	8165/8097
PG 1216+069	0.3313	0.1309	0.3078	69804	9184
3C 273	0.1580	0.1144	0.1417	18671	8017
PG 1259+593	0.4778	0.1144	0.4533	95760	8695
PKS 1302-102	0.2784	0.1183	0.2558	22119	8306
PG 1444+407	0.2673	0.1222	0.2442	48624	9184
3C 351.0	0.3719	0.1309	0.3483	73198	8015
PHL 1811	0.1917	0.1144	0.1690	33919	9418
H 1821+643	0.2970	0.1144	0.2741	50932	8165
Ton 28	0.3297	0.1231	0.3059	48401	9184

[a] The maximum redshift is defined for O VI absorbers at velocity separation > 5000 km s^{-1} from the background QSO, but the line search is conducted through the emission redshift of the QSO.

orders were continuum normalized and co-added to form a single, stacked spectrum using our own software. The continuum was determined using a low-order polynomial fit to spectral regions that are free of strong absorption features. The combined echelle spectra of 16 QSOs have on average $S/N > 7$ per pixel over the majority of the spectral regions covered by the data. Together the total redshift survey path length covered by the echelle sample is $\Delta z \approx 2.73$ over $z = [0.12, 0.5]$, comparable to the total redshift path length at $z < 0.15$, $\Delta z = 2.2$, carried out by Danforth & Shull (2005) toward 31 sightlines in FUSE spectra. Given the varying S/N versus wavelength along and between individual sightlines, we determine the Δz versus the O VI 1031 absorption equivalent width threshold W_0 in § 3.2.

3. A STATISTICAL SAMPLE OF O VI ABSORPTION SYSTEMS

3.1. *The Search for O VI Doublet Features*

To establish a statistically representative sample of O VI absorbers, we carry out a blind survey of O VI doublet features along each sightline that does not require known presence of hydrogen Lyα or other ionic transitions. Before conducting the doublet search in each QSO spectrum, we first exclude spectral regions of known absorption features from the Milky Way. Next, we search in the literature for known intervening absorbers, and further exclude spectral regions that contain these known features from the subsequent doublet search. For those sightlines not well studied, we performed this search ourselves. For the doublet search, we first smooth each stacked echelle spectrum using the Hanning function. Next, we step through the smoothed spectrum and search for deviant pixels that show negative fluctuation from unity by $> 1.5\,\sigma_c$, where σ_c is the 1-σ error per smoothed pixel. We then determine whether a deviant pixel is a candidate absorption line based on a single gaussian-profile fit to the negative fluctuation. We restrict the width of the model profile to be no less than the spectral resolution element and no larger than 300 km s^{-1}. The last criterion is justified based on the line width distribution of known O VI absorbers (Heckman et al. 2002; Danforth & Shull 2005). The deviant pixel is discarded from further consideration if the absorption equivalent width W based on the best-fit gaussian profile has $< 2\,\sigma$ significance.

Next, we treat each candidate absorption feature as the O VI 1031 line and determine the corresponding redshift. Then we examine whether the spectrum is consistent with the presence of both members of the O VI doublet based on a simultaneous doublet profile fit at the expected locations of the redshifted O VI 1031 and O VI 1037 lines. At this stage, we restrict both members to share the same line width and have a fiducial line ratio of 2 : 1, given the ratio of their respective oscillator strengths. The product of the doublet fitting procedure is a list of candidate O VI absorption doublets and their rest-frame absorption equivalent widths, $W_r(1031)$ and $W_r(1037)$. We visually examine every candidate and accept doublets that satisfy both of the following two criteria. First, the O VI 1031 line has $> 3\,\sigma$ significance. Second, the line ratio $R_{\rm O\,VI} \equiv W_r(1031)/W_r(1037)$ falls between $1 - \sigma_{R_{\rm O\,VI}}$ and $2 + 2\,\sigma_{R_{\rm O\,VI}}$, where $\sigma_{R_{\rm O\,VI}}$ is the associated measurement uncertainty in $R_{\rm O\,VI}$. Because the O VI 1031 transition is required to have at least 3-σ significance, the presence of both members together warrants a higher significance for the detection of each O VI doublet.

The entire sample of uncovered O VI absorbers include both foreground absorbers and absorbers that are associated with the host of the background QSOs. In the following discussion, we define a "random sample" that consists of absorbers with $|\Delta v| > 5000$ km s^{-1} from the background QSOs and an "associated sample" that are within $|\Delta v| < 5000$ km s^{-1} of the QSOs, where the ionization background is expected to be significantly different from the meta-galactic radiation field (e.g. Weymann et al. 1981). The results of our search are summarized in Table 2. For each QSO line of sight, we report in columns (2) through (4) the total number of random absorbers, the minimum absorption equivalent width of the uncovered absorbers on that sight-

line, $W_r^{\rm min}$, and the presence/absence of absorbers in the vicinity of the background QSO.

Figure 1 presents three examples of the O VI absorption doublet uncovered in our blind search (panels a–c), together with an example of a previously reported absorber that is not recovered in our search (panel d). While our search routine has uncovered 27 absorbers toward 16 random lines of sight, four of 16 systems previously reported toward seven lines of sight by other authors are not confirmed in our survey. We discuss these systems in more detail in § 5 and paper II. As a final step, we identify additional transitions associated with each fiducial O VI absorber. We perform a Voigt profile analysis to the O VI doublets, as well as Ly α, β (where available) using the VPFIT[3] software package. In cases where absorbers have a complex structure, we attempt a multiple-component model profile. Note that we consider absorption components with velocity separation $\Delta\, v \leq 200$ km s^{-1} as a single absorber in the statistical sample.

3.2. *Completeness of the Search*

To characterize the statistical properties of the O VI absorbers uncovered in our blind doublet search, it is necessary to first estimate the completeness of the survey. This is particularly important for the STIS data because (1) the S/N varies substantially across the entire wavelength range in each echelle spectrum and (2) individual QSO spectra were obtained from different programs and span a wide range in their mean noise levels. We perform a suite of Monte-Carlo simulations to quantify the completeness of our blind doublet search. A specific goal of the Monte-Carlo simulations is to estimate the total redshift path length $\Delta\, z$ covered by the survey for a given absorption equivalent width threshold in the O VI 1031 transition, W_*, over which absorbers of $W_r \geq W_*$ can be recovered. Exploring the completeness versus W_* allows us to maximize the survey efficiency, given the already small spectroscopic quasar sample.

To carry out the simulations, we first mask regions along a single sightline k that are blocked by strong Galactic or extra-galactic absorption (e.g. Galactic O I 1302, or Galactic and extra-galactic Ly α). Note that a strong absorption line at λ_x will render us insensitive to doublet features in *two* regions in redshift space ($\lambda_x/1031.927 - 1.0$ and $\lambda_x/1037.616 - 1.0$), since it may mask either member of the O VI doublet. Next, we step through the redshift space defined by $z_{\rm min}$ and $z_{\rm QSO}$ of the sightline defined in Table 1. At each redshift z_i, we adopt an intrinsic line width of $b = 10$ km s^{-1} (corresponding to a gas temperature of $T \sim 10^5$ K), generate a model absorption line of varying strength W_{in}, redshift the model to z_i, and perturb the smooth model within the random noise characterized by the 1-σ error array of the original echelle spectrum. Next, we apply the line search program and evaluate whether the synthetic absorption feature can be recovered. We repeat the procedure 1,000 times for each input line strength and determine the 3-σ detection threshold at $W_0^k(z_i)$, where the recovery rate of the synthetic absorption features is 99.7%. Finally, we repeat the procedure for all 16 QSO spectra in the echelle sample.

[3] http://www.ast.cam.ac.uk/ rfc/vpfit.html

The result of the Monte-Carlo simulations is a sensitivity curve $W_0^k(z)$ for every QSO sightline k that represents the 99.7% completeness of our blind O VI survey. These curves together allow us to calculate the total survey path length versus W_0 for the entire sample of O VI absorbers from our search. For absorbers of $W_r > W_0$, they are expected to be detected at greater than 3-σ confidence level. We present in Figure 2 the collective $W_0(z)$ curve from all 16 QSO sightlines together. At each redshift, the spread in W_0 represents varying spectral quality in the echelle spectra of different QSOs. The plot shows that our blind search is sensitive to $W_r \sim 30$ mÅ absorbers at $z \approx 0.2 - 0.5$, while at $z < 0.2$ the majority of the spectra are sensitive to absorbers of $W_r > 50$ mÅ.

To calculate the total survey path for our blind search, we first define a redshift path density $g(W_r, z)$ at z_i as

$$g(W_r, z_i) = \sum_k H(z_i - z^k_{\rm min})\, H(z^k_{\rm max})\, H(W_r - W_0^k(z_i)), \tag{1}$$

where H is the Heaviside step function, $[z^k_{\rm min}, z^k_{\rm max}]$ are the minimum and maximum redshifts observed for the kth QSO in Table 1, and the sum extends over all QSO sightlines in the echelle sample. The total redshift path length covered by the survey for a given equivalent width threshold W_r is therefore defined by

$$\Delta\, z\,(W_r) \equiv g(W_r) = \int g(W_r, z)\, dz. \tag{2}$$

We evaluate equations (1) and (2) based on a redshift interval of $\delta\, z = 0.0001$. The results are shown in panel (a) of Figure 3 for three different equivalent width thresholds, $W_r = 30, 50, 80$ mÅ. The plot illustrates that, as stronger absorber are considered, the total survey path length increases; and that weaker absorbers require higher signal-to-noise data. Several strong dips are immediately apparent at redshifts $z \approx 0.18, 0.21, 0.22, 0.26, 0.29$, which correspond to Galactic absorption from Ly α 1215, S II 1250, S II 1259, O I 1302, C II 1334 respectively.

In panel (b) of Figure 3, we show the redshift path along individual sightlines covered by our survey (solid black lines). Masked out regions due to Galactic absorption features (e.g. the Lyα 1215 transition) or other ionic transitions of known intervening absorbers appear as gaps in the path. Blue segments indicate the spectral regions that are sensitive to $W_r = 30$ mÅ. The tick-marks in panel (b) indicate the location of random O VI absorbers identified in our survey. We summarize the completeness of our O VI search in columns (5) and (6) of Table 2, where we list the total redshift path sensitive to $W_r = 30$ and 50 mÅ for each line of sight.

4. STATISTICAL PROPERTIES OF THE O VI ABSORBERS

We detect a total of 27 random O VI doublets along 16 QSO lines of sight over a redshift range from $z_{\rm O\,VI} = 0.12$ to $z_{\rm O\,VI} = 0.495$ with a mean redshift of $\langle z \rangle = 0.25$. Furthermore, we uncover associated absorbers toward nine QSOs at $|\Delta\, v| < 5000$ km s^{-1} from the background QSOs. The random O VI absorbers form a statistically representative sample for constraining their global mean properties. The associated O VI absorbers form a uniform sample for studying the gaseous halos of distant QSO hosts. Here we consider the statistical properties

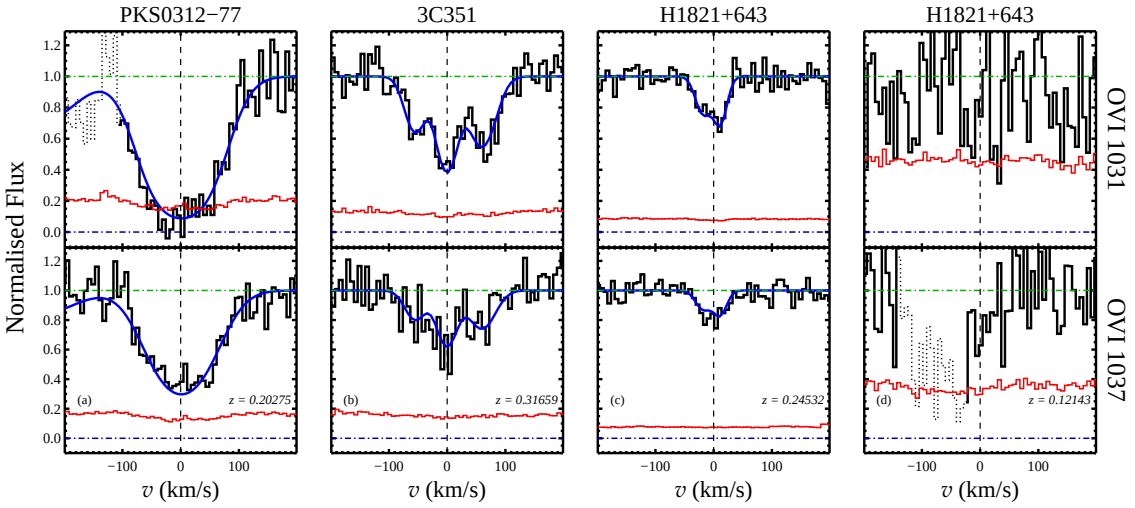

FIG. 1.— Examples of O VI doublets. For each doublet, the λ1031 member is plotted in the top panel and the associated λ1037 line at the bottom. The corresponding 1-σ error array is shown in orange. We also present a best-fit Voigt profile of each absorber in blue. The spectra have been binned by a factor of 2 for display only. In panels (a) and (b), we present new O VI absorbers uncovered at $z = 0.2028$ and $z = 0.3166$ in our search routine, along the sightlines toward PKS0312−77 and 3C351, respectively. In panel (c), we present a previously known absorber at $z = 0.24532$ toward H 1821+643 (Tripp et al. 2000) that has also been recovered in our blind search. Finally, we show in panel (d) an absorber previously reported by these same authors at $z = 0.1214$ toward H 1821+643 based on additional FUSE spectra of the QSO. It is clear that the quality of available STIS spectra does not allow us to recover this absorber. Our random sample therefore does not include this system.

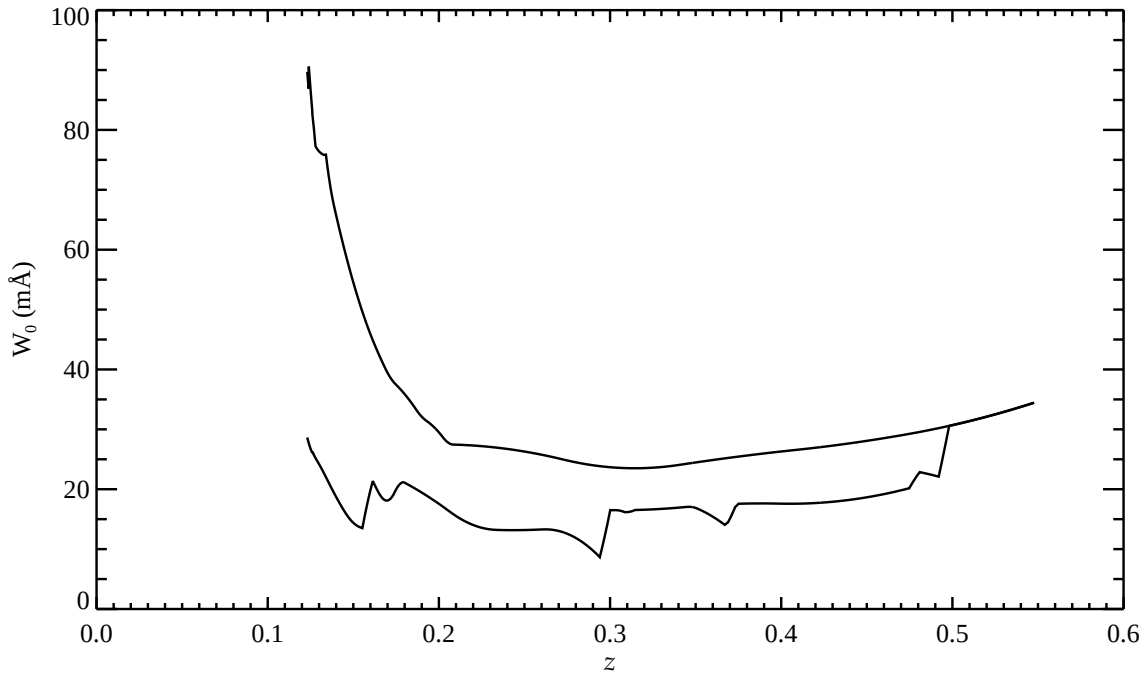

FIG. 2.— The 99.7% completeness limit in the absorption equivalent width, W_0, of the O VI 1031 transition versus redshift, for all 16 sightlines in the STIS echelle sample. At each redshift, the spread in W_0 represents varying spectral quality across different lines of sight. For absorbers at z_i with $W_r > W_0(z_i)$, they are expected to be detected at greater than 3-σ confidence level. The plot shows that the STIS echelle sample as a whole is most sensitive to $W_r \sim 30$ mÅ absorbers at $z \approx 0.2 - 0.5$. while at $z < 0.2$ the majority of the spectra are sensitive to absorbers of $W_r > 50$ mÅ.

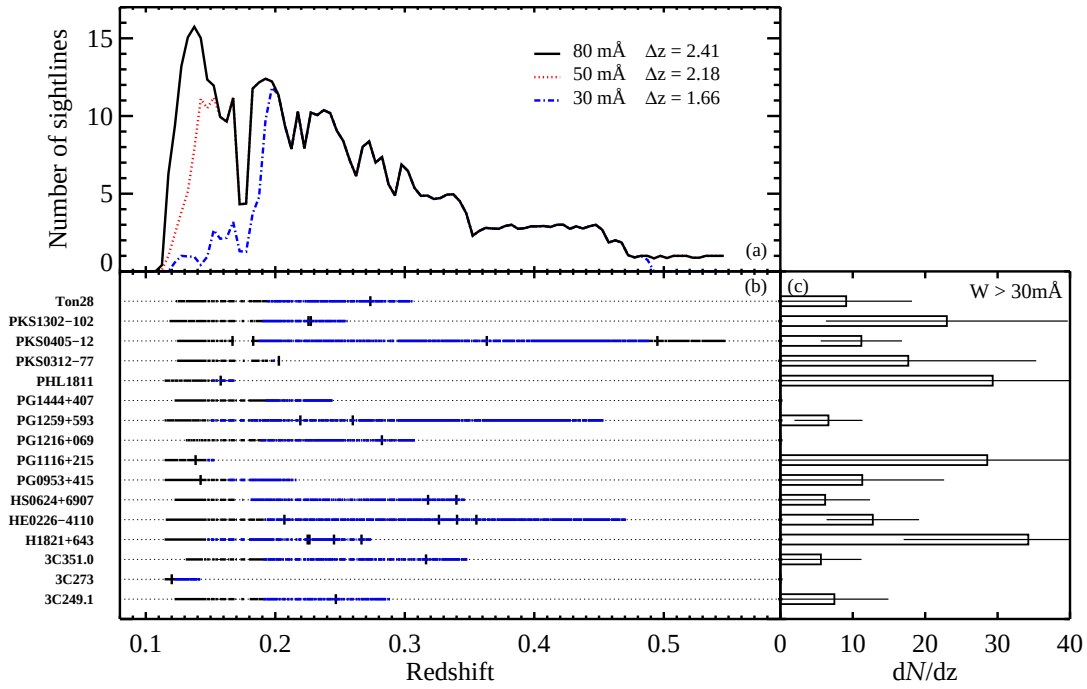

FIG. 3.— Summary of the results from our blind search of O VI absorbers. In Panel (a), we present the total redshift path covered by the entire sample of 16 sightlines for different absorption equivalent width thresholds W_*. Based on a series of Monte-Carlo simulations, we derive a total redshift path of $\Delta z = 1.66, 2.18$, and 2.42 for $W_r = 30, 50, 80$ mÅ, respectively. In panel (b), we show for each individual QSO sightline the total redshift path allowed by the STIS echelle spectrum (black solid lines) and the redshift path that is sufficiently sensitive for detecting a $W_r = 30$ mÅ absorber at $> 99.7\%$ confidence level (blue lines). In panel (c), we present the number density of $W_r \geq 30$ mÅ O VI absorbers per sightline evaluated based on individual lines of sight, together with their associated errors. The errors are estimated according to Equation (4). We see a significant variation across the 16 sightlines that cannot be easily accounted for by random errors.

TABLE 2
SUMMARY OF THE BLIND O VI SURVEY AND THE SURVEY LIMITS

QSO	$N_{\rm abs}^{\rm random}$	$W_r^{\rm min}$	Associated	Δz ($W \geq W_*$)		$d\mathcal{N}/dz$
			Absorbers	($W_* = 50$ mÅ)	($W_* = 30$ mÅ)	($W_* = 30$ mÅ)
(1)	(2)	(3)	(4)	(5)	(6)	(7)
HE 0226−4110[1,2,3]	4	43	Y	0.3055	0.2593	13 ± 7
PKS 0312−77	1	655	N	0.0375	0.0014	18 ± 18
PKS 0405−12[4,5]	4	30	N	0.3542	0.2780	12 ± 6
HS 0624+6907[6]	2	27	Y	0.1681	0.1458	6 ± 6
PG 0953+415[7,8]	1	121	Y	0.0698	0.0434	11 ± 11
3C 249.1	1	72	Y	0.1206	0.0826	8 ± 8
PG 1116+215[9,10]	1	76	Y	0.0307	0.0053	28 ± 28
PG 1216+069	1	26	N	0.1339	0.1047	0 ± 10
3C 273[11]	1	22	N	0.0271	0.0195	0 ± 51
PG 1259+593[12]	2	77	N	0.2851	0.2680	7 ± 5
PKS 1302−102	2	30	N	0.0992	0.0596	26 ± 19
PG 1444+407	0	...	Y	0.0927	0.0478	0 ± 21
3C 351.0[13]	1	232	Y	0.1575	0.1313	6 ± 6
PHL 1811[14]	1	64	Y	0.0388	0.0133	23 ± 23
H 1821+643[15]	4	30	Y	0.1226	0.0999	34 ± 17
Ton 28	1	26	Y	0.1396	0.0991	0 ± 10
total (16 sightlines)	27		10	2.18	1.66	10 ± 2

NOTE. — See also: (1) Lehner et al. (2006); (2) Savage et al. (2005); (3) Ganguly et al. (2006); (4) Chen & Prochaska (2000); (5) Prochaska et al. (2004); (6) Aracil et al. (2006); (7) Tripp & Savage (2000); (8) Savage et al. (2002); (9) Sembach et al. (2004); (10) Richter et al. (2006); (11) Heap et al. (2002); (12) Richter et al. (2004); (13) Yuan et al. (2002); (14) Jenkins et al. (2003); (15) Tripp et al. (2000).

of the two samples separately. Studies of the physical nature of individual absorbers will be presented in a separate paper (Thom & Chen 2008; Paper II).

4.1. *The Incidence of Random O VI Absorbers*

The Monte-Carlo simulations presented in § 3.2 allow us to estimate the total redshift path length as a function of absorption equivalent width, from which we can then derive an accurate estimate of the number density of O VI absorbers per line of sight, using individual sightlines separately or the entire QSO echelle sample collectively. For each absorber of rest-frame O VI 1031 absorption equivalent width $W_r^i > W_*$ identified in our search, the contribution to the total number density per line of sight $d\mathcal{N}/dz$ is $1/g(W_r^i)$. Over a statistical sample, we can therefore derive for a given equivalent width limit W_*,

$$d\mathcal{N}(W \geq W_*)/dz = \sum_i \frac{1}{\Delta\, z(W_r^i)} \times H(W_r^i - W_*) \quad (3)$$

where the sum extends over all systems found in a random sample and H is the Heaviside step function. Note that $\Delta\, z\,(W_r^i)$ varies with W_r^i. A stronger absorber may be detected in lower S/N spectra, allowing a larger survey path length for a given QSO echelle sample. Equation (3) is therefore not the total number of absorbers, $N_{\rm abs}^{\rm random}$, divided by a fixed path length, $(\Delta\, z)$. The variance of $\mathrm{d}\mathcal{N}/\mathrm{d}z$ is evaluated according to

$$\sigma^2_{d\mathcal{N}/dz} = \sum_i \frac{1}{[\Delta\, z(W_r^i)]^2} \times H(W_r^i - W_*). \quad (4)$$

We first evaluate $\mathrm{d}\mathcal{N}/\mathrm{d}z$ separately for individual lines of sight, adopting a common threshold for all QSO spectra. The results for $W_* = 30$ mÅ are summarized in column (7) of Table 2, and presented in panel (c) of Fig. 3. Despite the relatively short path length per line of sight, it is immediately apparent from Fig. 3 that there is a substantial variation in $\mathrm{d}\mathcal{N}/\mathrm{d}z$ from one line-of-sight to another. In contrast to the line-of-sight toward H 1821+643, along which four O VI absorbers are found over $\Delta\, z \lesssim 0.1$ (Tripp et al. 2000), we note that the sightlines toward HS 0624+6907, PG1259+593, and 3C 351.0 allow longer survey paths but exhibit fewer absorbers (between 1 and 2). The large scatter in $\mathrm{d}\mathcal{N}/\mathrm{d}z$ between random sightlines underscores the necessity of a statistically significant sample of O VI absorbers for an unbiased estimate of their incidence.

Combining all 16 QSO lines of sight together, we derive $d\mathcal{N}(W \geq 50\ \mathrm{mÅ})/dz = 6 \pm 3$ over $\Delta\, z\,(W_* = 50\ \mathrm{mÅ}) = 2.18$, and $d\mathcal{N}(W \geq 30\ \mathrm{mÅ})/dz = 9 \pm 4$ over $\Delta\, z\,(W_* = 30\ \mathrm{mÅ}) = 1.66$. In § 5 and panel (b) of Figure 5, we show that our number density measurements can be explained well by recent numerical simulations that do not require super starburst outflow, but account for non-equilibrium ionization conditions (Cen & Fang 2006).

4.2. *The Cosmological Mass Density of Ionized Gas*

A particularly interesting quantity to determine, based on a statistically representative O VI absorber sample, is the cosmological mean mass density contained in the O^{5+} ions, $\Omega_{\rm O^{5+}}$. In principle, we can then derive the cosmological mean mass density of warm baryons, $\Omega_{\rm b}$, probed by the O VI transition according to

$$\Omega_{\rm b} = \frac{1}{f}\,\frac{\mu}{Z \times (\mathrm{O/H})_\odot}\,\frac{m_{\rm H}}{m_{\rm O}}\,\Omega_{\rm O^{5+}}, \quad (5)$$

where $f \equiv N(\mathrm{O}^{5+})/N(\mathrm{O})$ is the fiducial ionization fraction of the O VI absorbing gas, $Z \equiv (\mathrm{O/H})/(\mathrm{O/H})_\odot$ represents its mean metallicity, $(\mathrm{O/H})_\odot$ is the solar oxygen to hydrogen ratio by number, μ is the mean atomic mass of the gas ($\mu = 1.3$ for gas of solar composition), and $m_{\rm H}$ and $m_{\rm O}$ are the atomic weight of hydrogen and oxygen, respectively. In the following calculation, we adopt $(\mathrm{O/H})_\odot = 4.57 \times 10^{-4}$ (Asplund et al. 2004).

Following Lanzetta et al. (1991), we calculate $\Omega_{\rm O^{5+}}$ according to

$$\Omega_{\rm O^{5+}} = \frac{H_0\, m_{\rm O}}{c\,\rho_c} \int N(\mathrm{O\,VI})\, f(N(\mathrm{O\,VI}))\, d\,N(\mathrm{O\,VI}) \quad (6)$$

$$= \frac{H_0\, m_{\rm O}}{c\,\rho_c} \sum_i \frac{N_i(\mathrm{O\,VI})}{\Delta\, X_i} \quad (7)$$

where ρ_c is the present-day critical density, $f(N(\mathrm{O\,VI}))$ is the frequency distribution function defined as the number of O VI absorbers per column density interval per unit absorption path-length, N_i is the corresponding O VI absorption column density for absorber i with rest-frame absorption equivalent width W_r^i and $\Delta\, X_i$ is the co-moving absorption path length covered by the entire echelle sample at the absorption strength W_r^i. The co-moving absorption path length $\Delta\, X_i$ for absorber i is related to the total redshift path length $\Delta\, z$ evaluated from Equation (2) at W_r^i according to

$$\frac{d\,X}{d\,z} = \frac{(1+z)^2}{[\Omega_M\,(1+z)^3 - (\Omega_M + \Omega_\Lambda - 1)(1+z)^2 + \Omega_\Lambda]^{1/2}}. \quad (8)$$

The corresponding 1-σ error is evaluated according to

$$\sigma_{\Omega_{\rm O^{5+}}} = \frac{H_0\, m_{\rm O}}{c\,\rho_c} \left[\sum_i \frac{\sigma^2_{N_i(\mathrm{O\,VI})}}{(\Delta\, X_i)^2}\right]^{1/2}. \quad (9)$$

For each uncovered absorber of W_r^i, we perform a Voigt profile fit to determine the corresponding N_i.

We present the frequency distribution function determined based on the random O VI absorber sample in panel (a) of Figure 5. The bin size is selected to contain roughly the same number of absorbers per bin. Error bars represent 1-σ Poisson fluctuations. For the sample of 23 random O VI absorbers with $W_r > 30$ mÅ, we therefore derive $\Omega(\mathrm{O}^{5+})\, h = (1.7 \pm 0.3) \times 10^{-7}$. Assuming a $Z = 1/10\, Z_\odot$ mean metallicity and $f = 0.2$ ionization fraction for the O VI gas, we further derive $\Omega_{\rm b} h \approx 0.0014$. Bearing in mind the large uncertainties in the metallicity and ionization fraction of the O^{5+} bearing gas, our derived mean mass density of ionized gas is less than 10% of the total baryon mass density (e.g. Burles et al. 2001).

4.3. *Associated O VI Absorbers*

We have excluded spectral regions within $|\Delta\, v| = 0-5000$ km s^{-1} from the background QSOs for establishing the statistical sample of random foreground absorbers in the previous discussion, due to potential contamination features from the QSO host environment. However, the blind O VI search has been carried out all the way through the emission redshifts of these QSOs. The O VI

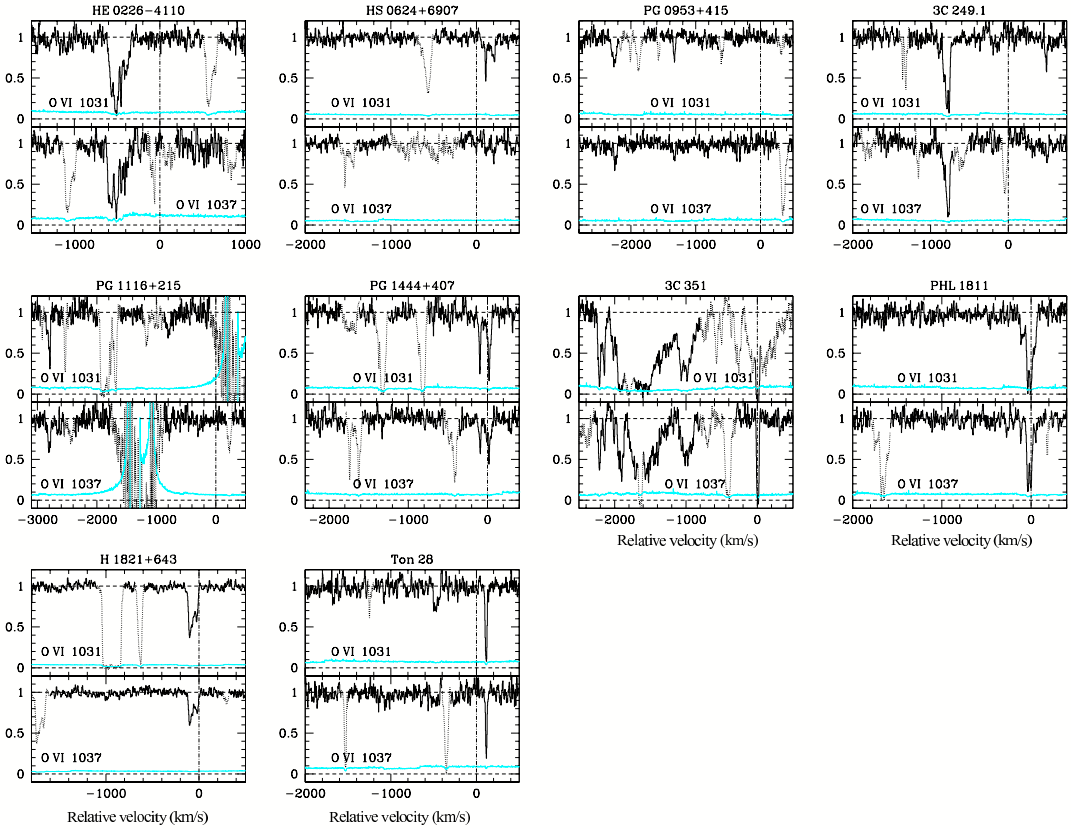

FIG. 4.— Absorption profiles of associated O VI absorbers identified in our STIS echelle sample.

absorbers found in the proximity of QSOs form a sample of associated absorbers that offers important constraints on the halo gas in QSO hosts (Chelouche et al. 2007, in prep).

Ten of the 16 QSOs in our STIS echelle sample exhibit strong O VI absorbers $|\Delta v| \leq 5000$ km s^{-1} blue-shifted from their emission redshifts (indicated in Table 2). We present the absorption profiles of these O VI absorbers in Figure 4. The rest-frame absorption equivalent width of the 1031 member ranges from $W_r = 60$ mÅ (the absorber at $\Delta v = -480$ km s^{-1} from Ton 28) to $W_r = 3$ Å (the multi-component absorber at $\Delta v \approx -1600$ km s^{-1} from 3C 351.0). The multi-component absorber found in the vicinity of 3C 351.0 has complex velocity profiles, extending from $\Delta v \approx 0$ km s^{-1} to $\Delta v \approx -2200$ km s^{-1}. It exhibits evidence of partial covering of the O^{5+} ions and is understood to originate in the outflow gas from the background QSO (Yuan et al. 2002).

Excluding the complex sightline toward 3C351.0, the total redshift path length defined within $|\Delta v| = 0 - 5000$ km s^{-1} blue-ward of the emission redshifts of the remaining 15 QSOs in our echelle sample is $\Delta z = 0.33$. At the equivalent width limit of our search $W_* = 50$ mÅ, we found nine O VI absorbers. We measure $d\mathcal{N}/dz = 27 \pm 9$ for O VI absorbers of $W_r(1031) > 50$ mÅ in the vicinity of background QSOs. This is significantly higher than the incidence of random absorbers in the foreground.

5. COMPARISONS WITH PREVIOUS SURVEYS

Our search in the STIS echelle QSO sample has uncovered a total of 27 random O VI absorbers of $W_r \gtrsim 25$ mÅ along 16 lines of sight, from which we derive the incidence of random O VI absorbers, $d\mathcal{N}(W \geq 30\ \text{mÅ})/dz = 10.4 \pm 2.2$ at $\langle z \rangle = 0.25$. This is roughly half of what is mentioned in Tripp et al. (2006), who reported a total of 44 O VI absorbers along 16 lines of sight and $d\mathcal{N}(W \geq 30\ \text{mÅ})/dz = 23 \pm 4$ at $z < 0.5$. An independent survey of O VI absorbers in known Lyα absorbers by Danforth & Shull (2005) yields an absorber frequency of $d\mathcal{N}(W \geq 30\ \text{mÅ})/dz = 17 \pm 3$ or $d\mathcal{N}(W \geq 50\ \text{mÅ})/dz = 9 \pm 2$ at $z < 0.15$. We present these different measurements in Figure 5, along with recent numerical simulation results that include galactic wind feedback and non-equilibrium ionization conditions (Cen & Fang 2006). It is interesting to note that models with starburst feedback are not required by our measurements.

The results of our blind search are consistent with those of Danforth & Shull (2005) from a FUSE survey at lower redshift that had been carried out in known Lyα absorbers. The agreement is qualitatively consistent with the small fraction of O VI absorbers that do not have an associated Lyα transition. The discrepancy between our results and those of Tripp et al. (2006) based on a similar set of QSO spectral sample is most puzzling. In the following, we discuss possible reasons for this discrepancy.

It is possible that the discrepancy is due to different QSO spectra covered by different surveys. Our random sample has been established based exclusively on available STIS echelle data. The sightline along H 1821+643

has the highest incidence of O VI absorbers of all 16 sightlines in our echelle sample (See Table 2 and the discussion in § 4.1). In addition to the four O VI absorbers originally reported in Tripp et al. (2000) and confirmed in our blind search, Tripp et al. (2001) reported an additional O VI absorber at $z = 0.1212$ in a targeted search in higher quality FUSE spectra. At $z = 0.1212$, the O VI λ1031 line is redshifted to $\lambda_{\rm obs} \approx 1157$ Å, where the sensitivity of STIS echelle declines steeply. The lack of sensitivity at the blue end of the echelle sample is accounted for by the completeness study of our random sample discussed in § 3.2. This $z = 0.1212$ absorber found in a targeted search after including additional FUSE spectra does not satisfy the criterion for establishing a statistically unbiased sample, and has therefore been excluded in our random sample.

In addition, there are O VI absorbers reported in the literature but not confirmed by our search. Along the same redshift path-length covered by our survey, 16 foreground O VI systems have been reported in the literature by other authors toward seven QSOs (HE 0226−4110, PKS 0405−123, PG 0953+415, PG 1116+215, PG1259+593, H 1821+643, and 3C 273; See Table 2 for corresponding references), four are not confirmed in our survey. An example is shown in panel (d) of Figure 1, where we show the spectral region of an O VI doublet along the sightline toward PG 1259+593 reported by Richter et al. (2004). The putative O VI 1031 member is blended with the Si III 1206 transition of a Lyα absorber at $z = 0.0461$ (the feature at $v = -30$ km s^{-1}) and the C III transition of a Lyα absorbers at $z = 0.2924$ (the feature at $v = +100$ km s^{-1}). Our search routine did not accept this absorber due to discrepant line strengths. Our random sample does not include this possible absorber. Along the same sightline, Richter et al. (2004) also reported the presence of an O VI absorber at $z = 0.3198$, which is not confirmed by our routine due to discrepant absorption profiles and an inconsistent line ratio.

Along the sightline toward HE 0226−4110, Lehner et al. (2006) reported five O VI absorbers with $W_r(1031) > 50$ mÅ. We cannot confirm the presence of their identification for a $z = 0.4266$ absorber. In particular, the putative feature identified as the O VI 1037 member is not present in our own reduction of the echelle spectra. Inspections of individual exposures showed that the broad feature are predominant in two of the 12 exposures, but the discrepancy may be due to different treatment in the hot pixels in echelle spectra (T. Tripp, private communication). Additional spectra obtained using the Cosmic Origin Spectrograph (COS) or STIS will be valuable for confirming the presence of the doublet. Consequently, this absorber is not included in our random sample.

6. DISCUSSION

6.1. *The Ionization State of the O VI Gas*

Various studies of individual O VI absorbers that consider both kinematic signatures of the absorption profiles and abundance ratios between different ions have concluded that a large fraction of these absorbers can be explained by a simple photo-ionization model (e.g. Tripp et al. 2000; Prochaska et al. 2004; Sembach et al. 2004; Lehner et al. 2006). These results are in contradiction to the expectation of a WHIM origin, under which the bulk of the O^{5+} ions originate in the shocks created as the gas accretes onto the large filamentary structures. However, it is often difficult to rule out a collisional ionization scenario for these absorbers. Additional uncertainties arise, if O VI absorbers arise in post-shock gas that is undergoing radiative cooling and a simple ionization equilibrium assumption does not apply (Gnat & Sternberg 2007).

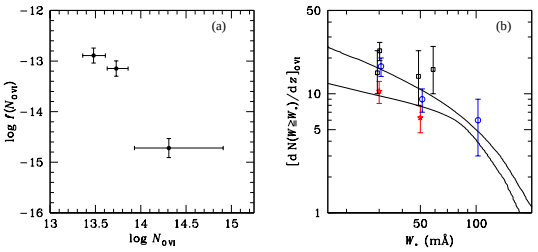

FIG. 5.— (a) The frequency distribution function of O VI absorbers from our random sample. The bin size is chosen for each bin to contain roughly the same number of absorbers. Error bars represents 1-σ Poisson fluctuations. (b) Observed incidence of O VI absorbers from different studies. Star points are from this work; open circles are from Danforth & Shull (2005) ; and open squares are from Savage et al. (2002); Prochaska et al. (2004); Tripp et al. (2006); Cooksey et al. (2008). Note that we have slightly offset the data points in the horizontal direction for clarification. The curves are recent WHIM predictions based on numerical simulations (Cen & Fang 2006) that account for non-equilibrium ionization conditions. The top curve further includes Galactic wind feedback.

The comparison of the absorption column densities in Figure 6 between Lyα and O VI transitions for the O VI selected sample (solid points) demonstrates that the N(H I) associated with these O VI absorbers spans nearly five orders of magnitude. In addition, stronger O VI transitions have on average stronger associated Lyα transitions. The null hypothesis in which Lyα and O VI column densities are randomly distributed among each other can be ruled out at $> 97\%$ confidence level based on a generalized Kendall test that considers the non-detection of Lyα for the O VI absorber at $z = 0.32639$ toward HE 0226−4110. We note that the STIS echelle sample is sensitive to O VI absorbers of $W_r > 80$ mÅ over the entire redshift path-length allowed by the data, and O VI absorbers of $W_r > 50$ mÅ over $\approx 80\%$ of the sightlines. The echelle spectra therefore allow us to uncover O VI absorbers of log N(O VI) > 13.5 over the majority of the sightlines. The correlation is therefore unlikely due to a selection bias. Including measurements from known O VI absorbers at low redshift (open squares and crosses), we find that the correlation remains at $> 80\%$ significance level.

The broad range of N(H I) spanned by these O VI absorbers also makes it difficult to apply a simple collisional ionization equilibrium model for explaining their origin. Furthermore, the correlation between N(O VI) and N(H I) indicates that the O VI absorbers appears to track closely H I gas in overdense regions, while the opposite does not apply (e.g. Danforth & Shull 2005). This trend can be understood under a simple photo-ionization scenario, and the slope in N(O VI) versus N(H I) implies a declining ionization parameter (defined as the number of ionizing photons per gas particle) with increasing gas

column density (see Figure 31 of Paper II).

6.2. *O VI Absorbers without Associated H I*

A unique feature of our blind search is that the finding of O VI doublet does not rely on known presence of Lyα transitions. The sample therefore allows us to constrain the fraction of O VI absorbers that do not show significant traces of H I. These absorbers may represent an extreme case for outflow gas that has been ejected into underdense regions by strong galactic winds (e.g. Kawata & Rauch 2007).

In Figure 6, we find that 26 of the 27 O VI absorbers in the random sample show associated H I absorption features. The only one possible Lyα-free system is found to have $N(\mathrm{O\,VI}) = 13.6 \pm 0.1$ at $z_{\mathrm{O\,VI}} = 0.3264$ toward HE 0226−4110 (the arrow in Figure 6). The comparison indicates that $< 5\%$ of O VI absorbers originate in underdense regions of $N(\mathrm{H\ I}) \lesssim 10^{13}$ cm^{-2} that are heavily metal-enriched by starburst outflows

6.3. *Large-scale Variation in Absorber Number Density*

Cosmological simulations also show that O VI absorbers originating in the WHIM reside in regions of over-density $\delta \equiv \rho/\langle\rho\rangle = 10 - 100$ at $z \sim 0$ (Davé et al. 2001; Cen et al. 2001; Fang & Bryan 2001). This is similar to what is found in simulation studies of Lyα forest absorbers, according to which by $z = 0$ the majority of Lyα absorbers are associated with $\delta = 10 - 100$. It is therefore interesting to examine the relation between Lyα and O VI absorbers.

Of the 16 QSO sightlines in our echelle sample, seven have been studied extensively for the line-of-sight properties of Lyα absorbers (Sembach et al. 2004; Williger et al. 2006; Lehner et al. 2006). We present in Figure 7 a comparison of the observed number densities between Lyα absorbers and O VI absorbers measured along individual sightlines. These include H 1821+643, HE 0226−4110, HS 0624+6907, PG 0953+415, PG 1116+215, PG 1259+593, and PKS 0405−123. The statistics of Lyα absorbers are taken from the compilation of Lehner et al. (2006). We have included the corrected Lyα absorber catalog for the PKS 0405−123 sightline. The error bars represent 1-σ uncertainties.

Considering all seven sightlines together, we find a mean number density of $\langle d\mathcal{N}/dz\rangle = 66$ for the Lyα absorbers with an r.m.s. dispersion of 15. In contrast, we find $\langle d\mathcal{N}/dz\rangle = 12$ for the O VI absorbers with an r.m.s. dispersion of 10. Examining the number density variation from one sightline to another, we find that the line of sight toward H 1821+643 with the highest incidence of O VI absorbers has the lowest incidence of Lyα absorbers. Figure 7 shows a possible inverse correlation between the number density of H I absorbers and the number density of O VI absorbers. While Lyα absorbers appear to be relatively more abundant than O VI along each sightline, the number density of O VI absorbers do not scale proportionally with the number density of Lyα absorbers along individual lines of sight.

This anti-correlation between $[d\mathcal{N}/dz]_{\mathrm{O\,VI}}$ and $[d\mathcal{N}/dz]_{\mathrm{Ly}\alpha}$ may be understood, if those sightlines with a higher incidence of O VI absorbers probe a larger fraction of more highly ionized regions. However, we note the result from § 6.1, where we find nearly every one of the O VI absorbers in our statistical sample shows an associated Lyα transition. On the other hand, if O VI absorbers originate preferentially in underdense regions, then a higher incidence of O VI implies a substantial fraction of the sightline probe underdense regions and hence a lower incidence of Lyα absorbers. This is expected if heavy elements from starburst outflows are ejected primarily into underdense regions (e.g. Kawata & Rauch 2007). Further insights can be obtained from a detailed examination of the large-scale galaxy environment of the O VI absorbers. A larger sample of QSO echelle spectra will also be valuable for a more quantitative study to confirm this result.

7. SUMMARY

We have conducted a systematic survey of intervening O VI absorbers in available echelle spectra obtained using HST/STIS with the E140M grating. We have collected echelle spectra of 16 distant QSOs from the HST data archive. These UV bright quasars at $z_{\mathrm{QSO}} = 0.17 - 0.57$ have been selected for HST/STIS observations by different authors for different studies, and represent a random, flux-limited sample of QSO echelle spectra for an unbiased search of intervening absorbers. The primary objectives of our blind O VI survey are: (1) to obtain a statistically representative sample of O VI absorbers along random lines of sight for an accurate measurement of the cosmological mass density of warm-hot gas at low redshift; and (2) to study the incidence of O VI absorbers along individual sightlines for quantifying the spatial variation of O VI absorbing gas.

Our search in the STIS echelle QSO sample has uncovered a total of 27 random ($|\Delta\, v| > 5000$ km s^{-1} from the background QSO) O VI absorbers with rest-frame absorption equivalent width of the 1031 member $W_r \gtrsim 25$ mÅ along 16 lines of sight. Ten of these QSOs also exhibit strong O VI absorbers at $|\Delta\, v| < 5000$ km s^{-1} blue-shifted from the QSO emission redshifts. Our O VI survey differs from previous studies in two fundamental ways. First, we do not require prior knowledge of the presence of other transitions such as Lyα. The echelle resolution allows us to identify the O VI absorption doublet based on their common line centroid and known flux ratio. Second, the survey completeness is well understood and characterized based on a series of Monte-Carlo simulations. We obtain an equivalent width threshold curve for every QSO sightline. Together, these curves allow us to estimate the total redshift survey path as a function of equivalent width threshold, thereby maximizing the survey efficiency at the limit allowed by the echelle spectra.

Based on the results of the Monte-Carlo simulations, we derive a total redshift path for random absorbers of $\Delta\, z = 1.66, 2.18$, and 2.42 for $W_r = 30, 50$ and 80 mÅ, respectively. The total path-length surveyed in our sample is comparable to the FUSE survey carried out at $z < 0.15$ by Danforth & Shull (2005), and is the largest at $z = 0.12 - 0.5$. The estimated total redshift path leads to a number density of $d\mathcal{N}(W \geq 50\ \mathrm{mÅ})/dz = 6.7 \pm 1.7$ and $d\mathcal{N}(W \geq 30\ \mathrm{mÅ})/dz = 10.4 \pm 2.2$. Recent numerical simulations that allow non-equilibrium ionization conditions explain the observations very well. In contrast, we also measure $d\mathcal{N}/dz = 27 \pm 9$ for O VI absorbers of

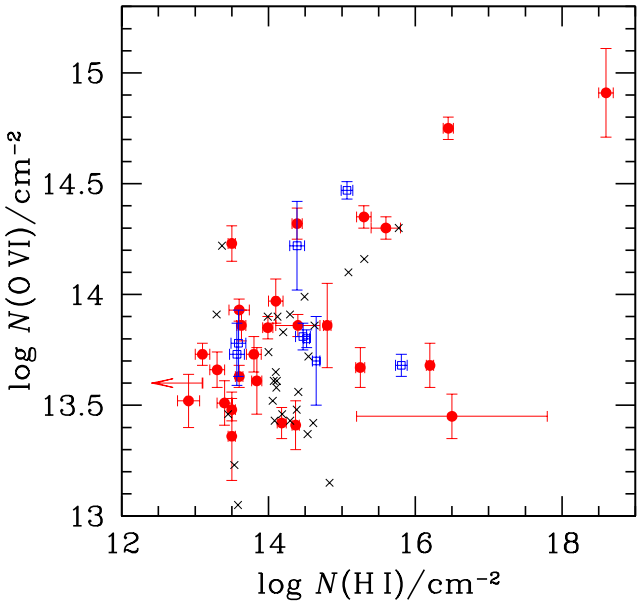

FIG. 6.— Comparison between N(O VI) and N(H I) for the 27 O VI absorbers identified in our blind search (solid points. All absorbers but one have an associated Lyα absorption line. We have also included published absorbers at low redshifts. Open squares are $z < 0.12$ absorbers presented in Savage et al. (2002) for PG 0953+415, in Sembach et al. (2004) for PG 1116+215, in Richter et al. (2004) fo PG 1259+593, in Prochaska et al. (2004) for PKS 0405−123, and in Cooksey et al. (2008) for PKS 1302−102. Crosses indicate measurements from a FUSE survey by Danforth & Shull (2005).

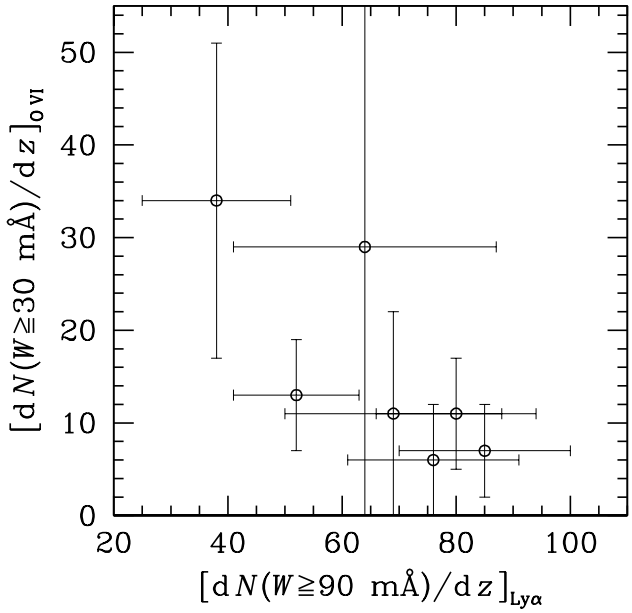

FIG. 7.— Comparison of the line density variation from one line of sight to another for hydrogen Lyα absorbers and O VI absorbers. The number density of Lyα absorbers measured for individual sightlines are taken from Lehner et al. (2007) for Lyα absorbers of rest-frame equivalent width W_r(Lyα) > 90 mÅ and the number density of O VI absorbers measured for individual sightlines are from the blind search for O VI absorbers of rest-frame equivalent width W_r(O VI) > 30 mÅ presented in this paper. We find a possible inverse correlation between the number density of H I absorbers and the number density of O VI absorbers.

$W_r(1031) > 50$ mÅ in the vicinity of background QSOs. For the sample of 27 random O VI absorbers, we further derive a mean cosmological mass density of the O VI ions $\Omega(O^{5+})\,h = (1.7 \pm 0.3) \times 10^{-7}$ that leads to a mean cosmological mass density of warm baryons $\Omega_b h \approx 0.0014$.

Using the statistical sample of O VI absorbers, we show that $< 5\%$ of O VI absorbers originate in underdense regions that do not show significant trace of H I. In addition, a comparison of the absorption column densities between Lyα and O VI transitions for the O VI selected sample shows that the N(H I) associated with these O VI absorbers spans nearly five orders of magnitude, making it difficult to apply a simple collisional ionization equilibrium model for explaining their origin. Furthermore, stronger O VI transitions have on average stronger associated Lyα transitions, indicating that the O VI absorbers appear to track closely H I gas in overdense regions, while the opposite does not apply. At the same time, comparisons of individual line-of-sight properties show a moderate inverse correlation between the number density of H I absorbers and the number density of O VI absorbers. While nearly all O VI absorbers have an associated Lyα transitions to $N(\mathrm{H\ I}) \gtrsim 10^{13}$ cm^{-2}, the presence of abundant O VI absorbers implies that a larger fraction of the gas along the line of sight becomes more ionized and therefore reducing the line density of Lyα absorbers. A larger sample of QSO echelle spectra is necessary for a more detailed study.

We thank N. Gnedin, J. X. Prochaska, and J. Tinker for valuable discussions. This research has made use of the NASA/IPAC Extragalactic Database (NED) which is operated by the Jet Propulsion Laboratory, California Institute of Technology, under contract with the National Aeronautics and Space Administration. C. T. and H.-W.C. acknowledges support from NASA grant NNG06GC36G. H.-W.C. acknowledges partial support from an NSF grant AST-0607510.

REFERENCES

Aloisi, A., van der Marel, R. P., Mack, J., Leitherer, C., Sirianni, M., & Tosi, M. 2005, ApJ, 631, L45
Aracil, B., Tripp, T. M., Bowen, D. V., Prochaska, J. X., Chen, H.-W., & Frye, B. L. 2006, MNRAS, 367, 139
Asplund, M., Grevesse, N., Sauval, A. J., Allende-Prieto, C., & Kiselman, D. 2004, A&A, 417, 751
Burles, S., Nollett, K. M., & Turner, M. S. 2001, ApJ, 552, L1
Burles, S. & Tytler, D. 1996, ApJ, 460, 584
Cen, R. & Fang, T. 2006, ApJ, 650, 573
Cen, R. & Ostriker, J. P. 1999, ApJ, 514, 1
Cen, R., Tripp, T. M., Ostriker, J. P., & Jenkins, E. B. 2001, ApJ, 559, L5
Chen, H.-W. & Prochaska, J. X. 2000, ApJ, 543, L9
Chen, X., Weinberg, D. H., Katz, N., & Davé, R. 2003, ApJ, 594, 42
Cooksey, K. L., Prochaska, J. X., Chen, H.-W., Mulchaey, J. S., & Weiner, B. J. 2008, ApJ, 676, 262
Danforth, C. W. & Shull, J. M. 2005, ApJ, 624, 555
Davé, R., et al. 2001, ApJ, 552, 473
Fang, T. & Bryan, G. L. 2001, ApJ, 561, L31
Fukugita, M., Hogan, C. J., & Peebles, P. J. E. 1998, ApJ, 503, 518
Ganguly, R., Sembach, K. R., Tripp, T. M., Savage, B. D., & Wakker, B. P. 2006, ApJ, 645, 868
Heap, S. R., Williger, G. M., Davé, R., Weymann, R. J., Jenkins, E. B., & Tripp, T. M., *Extragalactic Gas at Low Redshift*, edited by Mulchaey, J. S. & Stocke, J. 2002, vol. 254 of *Astronomical Society of the Pacific Conference Series*, 63–+
Heckman, T. M., Norman, C. A., Strickland, D. K., & Sembach, K. R. 2002, ApJ, 577, 691
Jenkins, E. B., Bowen, D. V., Tripp, T. M., Sembach, K. R., Leighly, K. M., Halpern, J. P., & Lauroesch, J. T. 2003, AJ, 125, 2824
Kawata, D. & Rauch, M. 2007, ArXiv e-prints, 704
Lanzetta, K. M., McMahon, R. G., Wolfe, A. M., Turnshek, D. A., Hazard, C., & Lu, L. 1991, ApJS, 77, 1
Lehner, N., Savage, B. D., Wakker, B. P., Sembach, K. R., & Tripp, T. M. 2006, ApJS, 164, 1
Mulchaey, J. S., Mushotzky, R. F., Burstein, D., & Davis, D. S. 1996, ApJ, 456, L5+
O'Meara, J. M., Burles, S., Prochaska, J. X., Prochter, G. E., Bernstein, R. A., & Burgess, K. M. 2006, ApJ, 649, L61
Persic, M. & Salucci, P. 1992, MNRAS, 258, 14P
Prochaska, J. X., Chen, H.-W., Howk, J. C., Weiner, B. J., & Mulchaey, J. 2004, ApJ, 617, 718
Rauch, M., et al. 1997, ApJ, 489, 7
Richter, P., Savage, B. D., Sembach, K. R., & Tripp, T. M. 2006, A&A, 445, 827
Richter, P., Savage, B. D., Tripp, T. M., & Sembach, K. R. 2004, ApJS, 153, 165
Savage, B. D., Lehner, N., Wakker, B. P., Sembach, K. R., & Tripp, T. M. 2005, ApJ, 626, 776
Savage, B. D., Sembach, K. R., Tripp, T. M., & Richter, P. 2002, ApJ, 564, 631
Sembach, K. R., Tripp, T. M., Savage, B. D., & Richter, P. 2004, ApJS, 155, 351
Spergel, D. N., et al. 2003, ApJS, 148, 175
Thom, C. & Chen, H.-W. 2008, ApJS, submitted (paper II)
Tripp, T. M., Bowen, D. V., Sembach, K. R., Jenkins, E. B., Savage, B. D., & Richter, P., *Astrophysics in the Far Ultraviolet: Five Years of Discovery with FUSE*, edited by Sonneborn, G., Moos, H. W., & Andersson, B.-G. 2006, vol. 348 of *Astronomical Society of the Pacific Conference Series*, 341–+
Tripp, T. M., Giroux, M. L., Stocke, J. T., Tumlinson, J., & Oegerle, W. R. 2001, ApJ, 563, 724
Tripp, T. M. & Savage, B. D. 2000, ApJ, 542, 42
Tripp, T. M., Savage, B. D., & Jenkins, E. B. 2000, ApJ, 534, L1
Verner, D. A., Tytler, D., & Barthel, P. D. 1994, ApJ, 430, 186
Wang, X., Tegmark, M., Jain, B., & Zaldarriaga, M. 2003, Phys. Rev. D, 68, 123001
Weymann, R. J., Carswell, R. F., & Smith, M. G. 1981, ARA&A, 19, 41
Williger, G. M., Heap, S. R., Weymann, R. J., Davé, R., Ellingson, E., Carswell, R. F., Tripp, T. M., & Jenkins, E. B. 2006, ApJ, 636, 631
Yuan, Q., Green, R. F., Brotherton, M., Tripp, T. M., Kaiser, M. E., & Kriss, G. A. 2002, ApJ, 575, 687